Vrije Universiteit Brussel

VRIJE UNIVERSITEIT BRUSSEL

Molecular Characterization of Bonding Interactions at the Buried Steel Oxide-Aminopropyl Triethoxysilane Interface Accessed by Ar Cluster Sputtering

Marcoen, Kristof; Gauvin, Mélanie; De Strycker, Joost; Terryn, Herman; Hauffman, Tom

Link to publication

Molecular Characterization of Bonding Interactions at the Buried Steel Oxide – Aminopropyl Triethoxysilane Interface accessed by Ar Cluster Sputtering

Kristof Marcoen,*,† Mélanie Gauvin,‡ Joost De Strycker,‡ Herman Terryn,†,¶ and Tom Hauffman†

†Vrije Universiteit Brussel, Research Group of Electrochemical and Surface Engineering (SURF), Pleinlaan 2, 1050 Brussels, Belgium

‡OCAS NV, President John F. Kennedylaan 3, 9060 Zelzate, Belgium

¶Delft University of Technology, Department of Materials Science and Engineering, Mekelweg 2, 2628 CD Delft, The Netherlands

E-mail: kristof.marcoen@vub.be

Abstract

The overall performance of any organic coating system on a metal is largely dependent on the primer coating which has the crucial function to ensure adhesion to the metal substrate. Although performance in terms of adhesion can be empirically measured, the underlying chemical adhesion mechanism is difficult to unravel. A detailed molecular characterization of interfacial chemistry is required for this purpose, but brings up the challenge to reach the buried interface without inducing excessive damage to its molecular structure. In this work, argon gas cluster ions are being applied to sputter through an aminosilane coating on steel, in order to access the steel oxide –

1

silane interface with time-of-flight secondary ion mass spectrometry (ToF-SIMS). In-situ atomic force microscopy (AFM) measurements during the sputter process demonstrate the importance of optimizing the Ar gas cluster ion beam in order to minimize sputter induced roughness and molecular damage. ToF-SIMS spectra obtained at the buried steel oxide – aminosilane interface accessed by sputtering were compared to spectra from a steel oxide – aminosilane interface that was directly accessible without the need for sputtering. This comparison allowed to identify contributions from sputter induced damage in the buried interface spectra. Fragments characteristic for interfacial bonding interactions could be extracted, although there is a significant loss of molecular information due to sputtering. Nevertheless, insights on the role of steel surface hydroxyl groups in the adsorption mechanism of aminosilanes could be obtained through deuteration of the steel substrate.

1   Introduction

Organic coatings are generally applied to metal substrates in a wide range of industries (construction, aerospace, automotive, packaging, biomedical healthcare, etc.) and usually consist of a topcoat and a primer coating. Topcoats are designed to provide application-oriented functionalities, whereas the role of a primer coating is universally threefold. In the first place, primer coatings must ensure adhesion to the metal substrate. Secondly, they act as barriers against corrosive substances in the environment, and third, they can be loaded with corrosion inhibitor additives to provide active corrosion protection when the coating is damaged. As such, the performance of a primer coating can be evaluated in terms of corrosion protection or in terms of adhesion. In order to enhance adhesion between the primer coating and metal substrate, metal substrates are subjected to certain pre-treatments. Classic pre-treatments on (galvanized) steel involve chromate conversion coating and zinc phosphating, but these processes are nowadays being replaced by healthier and greener alternatives. One alternative, which gained a lot of interest, is found in the application of organosilanes as

coupling agents that can be tailored to provide good adhesion to metal substrates, as well as to a variety of organic coatings.[1] The effectiveness of coatings in terms of adhesion can be evaluated by standardized peel or pull-off tests.[2] Although such adhesion tests can indicate whether a varying industrial process parameter leads to improved adhesion or not,[3] these measurements do not provide a thorough understanding of underlying bonding mechanisms. A molecular characterization of interfacial chemistry is required for this purpose, but not easily achieved. Evidence for interfacial bonding at the metal oxide – silane interface has been scarcely provided by XPS and infrared-based spectroscopy techniques.[4] ToF-SIMS turns out much more successful for the characterization of these systems.[5–7] In our previous work, thin films (< 5 nm) of aminopropyl triethoxysilane (APS) (Figure 1) were applied to a steel substrate, such that the APS-steel interface could be directly analyzed by surface sensitive analysis techniques. A successful characterization by ToF-SIMS showed that APS interacts with the steel substrate through silanol-steel interactions and amine-steel interactions.[8] Furthermore, through deuteration of steel surface hydroxyl groups, direct evidence for hydrogen bond interactions between silanol groups and steel surface hydroxyl groups was provided for the first time.[8] In general, the 'direct interface analysis' approach has been applied multiple times in literature as a successful strategy to obtain mechanistic insights on the adsorption of organics (carboxylic acids, amines, amides and isocyanates, ...) and (hybrid) organosilanes to a range of metal oxides.[8–15] Although this approach does provide valuable mechanistic insights on interfacial bonding, ultrathin organic films cannot fully represent commercial multicomponent (silane or polymer) coatings which contain additives and various binding agents.

$$C_2H_5\!-\!O$$
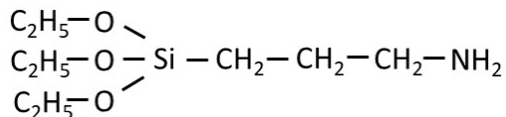$$C_2H_5\!-\!O-Si-CH_2-CH_2-CH_2-NH_2$$
$$C_2H_5\!-\!O$$

Figure 1: Molecular structure of aminopropyl triethoxysilane (APS).

The main difficulty for a characterization of the organic-inorganic interface is to find an ap-

proach to expose this buried interface without severely altering or destroying its molecular structure. Early approaches in literature employ mechanical methods such as ball cratering to expose the metal substrate,[16] but suffer from limitations that involve smearing of soft polymeric materials. A more successful approach, introduced by Watts et al. at the University of Surrey, implies taper sectioning of samples by ultra-low angle microtomy (ULAM).[17] ULAM makes use of a tungsten carbide microtome (an instrument frequently used in histology labs to cut extremely thin slices of materials) to expose the metal oxide-polymer interface.[14,18] Unfortunately, this method is limited to the use of thin (< 100 µm) metal foils as substrate material and therefore not applicable to industrial samples.

In view of analyzing industrial systems, a large interest goes out to sputter depth profiling with ion beams. Early studies already made use of monoatomic ion sources (e.g., Ar^+) to sputter through organic coatings, but were restricted to extract information from elemental depth profiles[16,19] as organic structures rapidly lose their molecular identity through accumulation of sputter induced damage. The advent of polyatomic ion sources has triggered an enormous progress in the last twenty years, enabling molecular depth profiling of organic materials.[20,21] Its success has been explained by molecular dynamics simulations which demonstrate that damage induced by polyatomic primary ions is confined to smaller volumes near the surface and sputter yields are significantly enhanced.[22,23] Among polyatomic ion sources, argon gas cluster ions are considered to be the most efficient and versatile projectiles for depth profiling of organics.[24–26] Large differences in sputter yield displayed by Ar clusters on organic and inorganic materials (organics are sputtered much faster[27]) provide the maximum opportunity to study organic-inorganic interfaces buried under organic coatings.[28] Nowadays, besides the high interest for polyatomic ion sources, a large interest goes out as well to low energy Cs^+ depth profiling, especially on multilayer hybrid materials, as low energy Cs^+ beams are shown capable to profile organic and inorganic materials with comparable erosion rates.[29,30]

Although a vast amount of research is available on the performance of Ar GCIBs and Cs^+

beams in terms of depth profiling on a variety of organics[20,27,30,31] and some studies have focused on resolving buried hybrid organic-inorganic interfaces,[28,29,32] no study in literature so far has discussed the feasibility to characterize molecular bonding interactions at buried hybrid interfaces accessed by sputtering. In this work, APS coatings on steel are sputtered by Ar cluster ions in order to expose the steel oxide – silane interface for a molecular characterization by ToF-SIMS. The steel oxide-APS interface is industrially relevant, since APS is commonly applied in commercial coating formulations in order to provide good adhesion to polyurethane and polyester coatings.[33] First focus will be on the fine-tuning of depth profiling conditions to APS coatings. This optimization process deserves special attention, as organosilanes tend to form three-dimensional siloxane (Si-O-Si) cross-linked structures which are inorganic in nature.[33] Sputter conditions are optimized in view of minimizing molecular damage induced by sputtering and atomic force microscopy (AFM) measurements are performed during the sputter process to evaluate sputter induced roughness. The buried steel oxide – APS interface accessed by sputtering was characterized by ToF-SIMS and compared to spectra obtained from a steel oxide – APS interface that was directly accessible without sputtering. Fragments characteristic for molecular interactions at the interface are evaluated in terms of possible influence from sputter induced damage and lead to mechanistic insights on interfacial bonding.

2 Experimental

2.1 Silane solution preparation

2v% and 20v% silane solutions were prepared at room temperature by adding APS (99 atom. %, Sigma-Aldrich) to a solvent mixture of milli-Q water and methanol ($\geq$ 99.5 atom. %, VWR Chemicals). A 90/10 (v%/v%) water/methanol ratio was chosen, based on a study by Ghosh et al. that evaluated the solvent composition with respect to solution stability and adhesion performance on stainless steel.[3] Wet deposition took place after 1 hour of hydrolysis

under continuous stirring. The silane solutions were used at their natural alkaline pH (10.4) during the deposition.

2.2 Substrate preparation

Low alloy cold rolled steel sheets with a thickness of 500 µm were cut into substrates of 1.5 x 1.5 cm^2 and subsequently polished with diamond paste to 0.1 µm roughness. Substrates were cleaned in an ultrasonic bath of ethanol and rinsed with ethanol and milliQ water. Next step was an alkaline treatment for 10 minutes, either in an 80 wt.% NaOH solution or in a 40 wt.% sodium deuteroxide solution (40 wt.% NaOD in D$_2$O (99.5 atom. % D), Sigma-Aldrich), at 70°C in order to form a surface hydroxide layer. In the end, substrates were rinsed with milliQ water and dried with N$_2$. The elemental composition of the steel sheets is provided in Table 1.

Table 1: Elemental composition of the steel substrate, determined by spark source optical emission spectroscopy.

	Value [m%]	St. dev.
Al	0.043	0.001
As	0.0010	<0.0001
B	<0.0010	NA
C	0.0062	0.0007
Co	0.0060	0.0001
Cr	0.0129	0.0002
Cu	0.0213	0.0006
Mn	0.128	0.001
Mo	0.0027	0.0001
Nb	0.0016	0.0002
Ni	0.0234	0.0001
P	0.0061	<0.0001
S	0.0092	<0.0001
Si	0.0060	0.0001
Sn	<0.0015	NA
Ti	0.055	<0.001
V	0.0022	0.0002

2.3   Silane deposition

Ultrathin ($<$ 5 nm) APS films were deposited from a 2v% silane solution by immersion of the steel substrate in the solution for 15 minutes. After immersion, samples were rinsed with water and dried with N_2. APS coatings with thicknesses in the range of 100 nm $-$ 1 µm were deposited from a 20v% APS solution by spin coating, using a WS-650 series spin coater from Laurell Technologies (North-Wales, USA). Spin-coating conditions for preparation of APS coatings of 900 nm and 300 nm thickness are provided in Table 2. The procedure comprises four steps: pre-deposition, deposition, spread and drying. The most important parameter that affects the final coating thickness for any precursor solution is the rotation speed during deposition and spread. Faster rotation speeds lead to lower thicknesses, as demonstrated in Table 2. Acceleration rates were chosen such that the peak spin-speed during the spread is reached within 2s.

Table 2: Spin-coating conditions to obtain APS coatings on steel coupons from a 20v% APS solution.

	time [s]	Rotation [rpm]	Acceleration [rpm/s]
900 nm APS coating			
pre-deposition	5	250	250
deposition	2.5	250	250
spread	10	500	250
dry	30	1000	500
300 nm APS coating			
pre-deposition	5	500	500
deposition	2.5	750	500
spread	10	1000	500
dry	30	2000	500

2.4   ToF-SIMS measurements

ToF-SIMS measurements were performed with a TOF.SIMS 5 system from ION-TOF GmbH (Münster, Germany), using a 30 keV Bi_3^+ primary ion beam operated in the high current bunched mode for high mass resolution (approximately 8000 at 29 u ($^{29}Si^+$)). The lateral

resolution achieved in high current bunched mode is $3\mu m$. The pulsed ion beam target current was approximately 0.70 pA. Positive ion mass spectra were acquired over a mass range of 1–800 u and calibrated using a list of fragments of known composition, such as Si^+, NH_3^+, CH_3O^+, $C_4H_5^+$, $SiOFe^+$, Fe_2^+, $Fe_2O_2H_2^+$ and $Fe_3O_3^+$. The accuracy of a mass assignment (in ppm) is calculated by taking the absolute difference between the experimental and theoretical mass of a fragment and dividing this number by the experimental mass. Depth profiles were obtained in dual beam configuration, where a 5 keV or a 10 keV Ar_{1200}^+ cluster ion beam was used as a sputter beam and Bi_3^+ was used to analyze the crater bottom. The sputter raster was $300\mu m \times 300\mu m$. A smaller analysis raster of $100\mu m \times 100\mu m$ was chosen in the center of the crater. Samples were mounted on a glass slide, to prevent a spectrum shift, which may occur when sputtering through an organic coating towards a metallic substrate, due to differential charging.

2.5   AFM measurements

AFM measurements were performed using the VLS-80 system from Nanoscan AG (Zürich, Switzerland). The VLS-80 combines high vacuum SPM with high precision sample navigation. The VLS-80 system is implemented in the TOF.SIMS 5 system and allows for a fast and accurate determination of sputter rates. AFM line scans can be obtained across the sputter crater, before and after sputtering. The crater depth difference before and after sputtering will be used to determine sputter rates and coating thicknesses. On the other hand, sputter induced roughness can be evaluated. NANOSENSORS™ PPP-NCLR AFM probes are employed in tapping mode to characterize sputter craters formed in organic coatings. The silicon tip is characterized by a guaranteed tip radius of curvature less than 10 nm, and a tip height of 10-15 µm. A 30 nm thick Al coating on the detector side of the cantilever enhances the reflectivity of the laser beam by a factor of about 2.5. The length of the cantilever is 225 µm and its resonance frequency is 190 kHz.

2.6 Multivariate analysis methods

ToF-SIMS mass spectra contain thousands of peaks representing secondary ion fragments. Peak intensities are the main variables in a ToF-SIMS dataset and show a large degree of correlation, since several secondary ion fragments can be generated from the same parent molecule. Multivariate analysis (MVA) methods are therefore particularly suited for application to a ToF-SIMS dataset.

Variables in a ToF-SIMS depth profile dataset are the peak intensities obtained at different depth levels. A set of n peaks for which intensities are acquired at m depth levels can be represented by a m x n data matrix $\mathbf{M}$. Matrix $\mathbf{M}$ is the input for a non-negative matrix factorization (NMF) analysis in which $\mathbf{M}$ is approximately factorized ($\mathbf{M} \approx \mathbf{HW}$) into non-negative matrices $\mathbf{H}$ and $\mathbf{W}$. $\mathbf{H}$ defines the fingerprint spectra of a defined number of components present in the depth profile and $\mathbf{W}$ represents the 'concentrations' of these compounds in function of depth (or sputter dose). The non-negativity of the NMF output, a main constraint of the technique, can be considered a natural choice since negative values make no physical or chemical sense for analytical chemistry data. One should bear in mind that NMF provides an approximate solution; appropriate algorithms and constraints must be applied in this iterative process to come to the best possible solution.[34] NMF performed in this work made use of a multiplicative update algorithm with a mean squared error objective function, originally created by Lee and Seung,[35] with the modifications suggested by Berry et al.[36] ToF-SIMS input data is pre-processed in two steps: (i) normalization of all ion peak intensities to total ion intensity, and (ii) Poisson scaling of the peak intensities according to a method proposed in literature.[37]

An important constraint that needs to be pre-defined for NMF is the number of components that are present in the depth profile.[38] Principal component analysis (PCA) is employed prior to NMF, as an exploratory tool to identify the different chemistries along the depth profile. Discussion and results for the PCA analysis can be found in the supplementary information. NMF and PCA analysis were performed using the simsMVA MATLAB app

(http://mvatools.com) developed by Trindade et al.[34]

3 Results and discussion

3.1 Optimization of depth profiling conditions on APS coatings

An argon gas cluster ion beam (GCIB) is applied to sputter through a spin-coated APS coating on steel in order to analyze the buried steel oxide – APS interface with ToF-SIMS. As there is no interest to profile through the steel substrate, depth profiling conditions should be optimized solely to sputter through the APS coating. Both cluster size and acceleration energy can be adjusted for Ar cluster projectiles. Figure 2a and b show ToF-SIMS depth profiles obtained with acceleration energies of 5 keV and 10 keV, respectively. Given that the argon cluster size is fixed to n = 1200, the energy-per-atom values (E/n) are 4.2 eV/atom and 8.3 eV/atom, respectively. Ion intensities are plotted for $^{30}Si^+$, Si_2NO^+, NH_3^+ and $C_3H_8N^+$. At the start of each profile, secondary ion intensities vary rapidly. This region is typically referred to as the transient region and is attributed to the fact that the concentration of molecules in the altered surface layer is determined by a balance between the resupply of molecules from the bulk, sputter induced damage and the removal of both intact and damaged species.[20] Besides the influence of sputtering, rapidly varying intensities can also be attributed to a difference in chemistry between surface and bulk material, and the presence of surface contamination.

A steady state region is reached in both profiles when the $^{30}Si^+$ intensity reaches a plateau. For pure materials, secondary ion intensities in the steady state region are not expected to change unless there is a change in sputtering yield.[20] It is remarkable that the $C_3H_8N^+$ intensity, which represents the organofunctional group of APS (Figure 1), reaches a plateau with the 10 keV settings, but keeps decreasing with the 5 keV settings and disappears after 800 s of sputtering (sputter dose 2.2 x 10^{16} ions/cm^2). This indicates that there is loss of molecular information due to accumulation of sputter induced damage. Si_2NO^+, on the other

hand, is a fragment that is typically not present in the mass spectrum of APS coatings and is likely representative for the damage caused by sputtering. This assumption is confirmed by comparing both Si_2NO^+ profiles. While the Si_2NO^+ reaches a plateau in the 10 keV profile quite fast, the Si_2NO^+ intensity keeps increasing in the 5 keV profile up to 2000 s (sputter dose 5.4 x 10^{16} ions/cm^2).

An AFM module implemented in the ToF-SIMS chamber allows for a fast and accurate determination of sputter rates and has been employed in the optimization of depth profiling conditions. Figure 2c-d shows AFM line scans obtained across the sputter crater, before and after sputtering, for the 5 keV profile and the 10 keV profile, respectively. Remarkably, the 5 keV settings resulted in a significant amount of sputter induced roughness, while under the 10 keV settings, the sample topography is largely retained. This can be explained by a threshold energy level that has to be exceeded in order to remove material efficiently. It seems that the threshold energy on APS coatings situates in the vicinity of 4 eV/atom. This value is significantly higher than the values usually reported on organic materials (below 1 eV/atom on HTM-1, NPB and Irganox 1010 according to Niehuis et al.[39]), which may be attributed to the partial inorganic nature of organosilane coatings. Depth profiling conditions were optimized in this section to sputter through an APS coating with retention of molecular information. A 10 keV Ar_{1200}^+ ion beam will be further applied for a buried interface analysis. It can be expected that the sputter rate drops several orders of magnitude once the steel substrate is reached. In any case, there is no need to optimize the sputter conditions based on the sputter rate difference between the organic coating and the metallic substrate, since our interest is only directed towards the hybrid interface.

In industrial coatings, which contain multiple polymeric components and additives, one should consider that, due to surface and interface segregation effects, the coating properties near the interface may be different from the bulk coating. In such a case, it might be necessary to provide additional optimization for depth profiling of the coating near the interface. However, in this study, a simple model coating of APS is applied. It can be

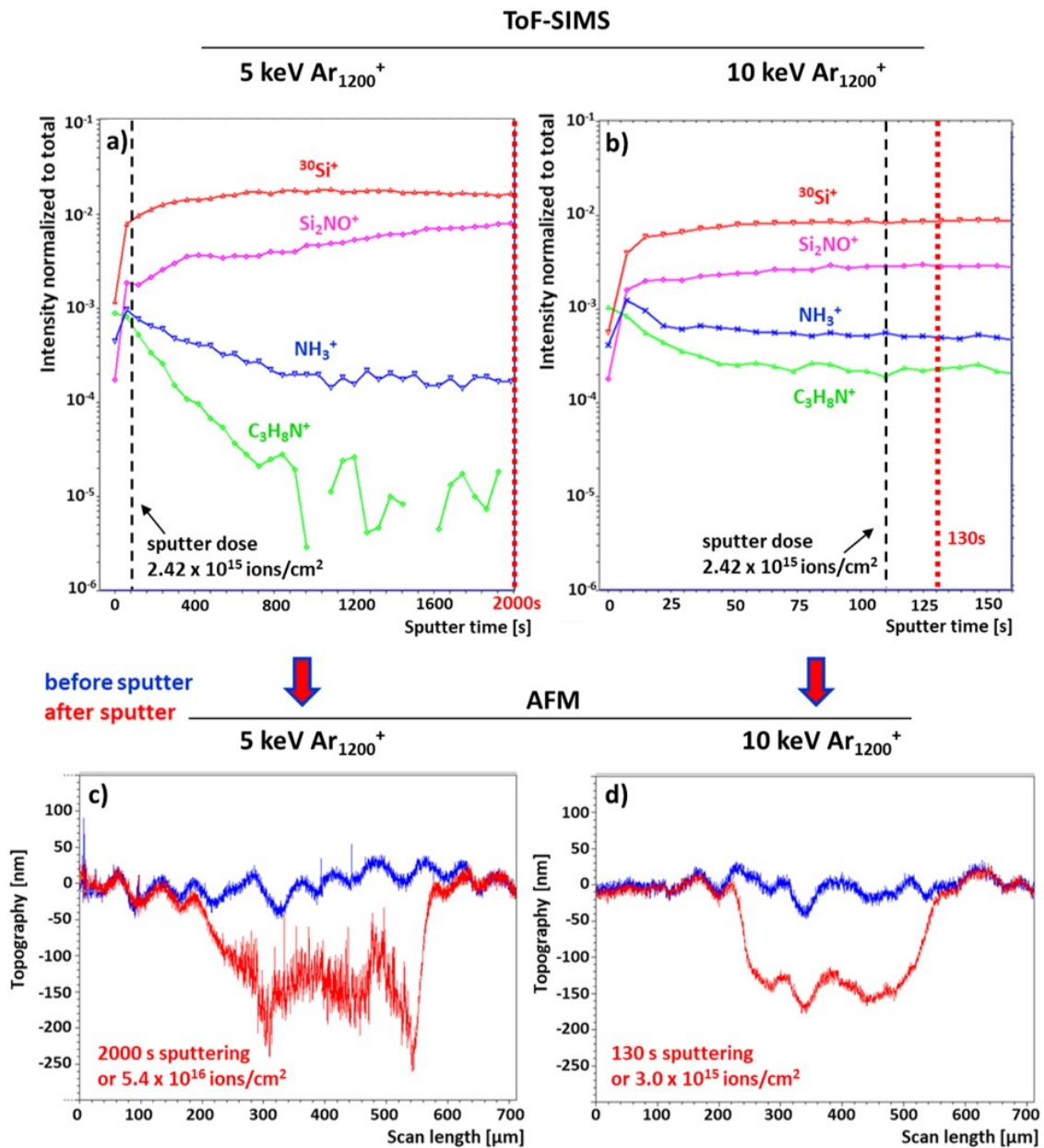assumed that additional optimization is not necessary.

Figure 2: (a) Depth profile of an APS coating obtained with a 5keV Ar_{1200}^+ ion beam. (b) Depth profile of an APS coating obtained with a 10keV Ar_{1200}^+ ion beam. (c) AFM linescan across the crater region before and after profiling with a 5 keV Ar_{1200}^+ ion beam (d) AFM linescan across the crater region before and after profiling with a 10 keV Ar_{1200}^+ beam.

3.2 Depth profiling and NMF analysis to expose the buried interface

Figure 3 shows a depth profile that goes through an APS coating towards the steel substrate. The dashed line at a sputter dose of 2.42 x 10^{15} ions/cm^2 marks a point in the steady state region of the depth profile, well beyond the transient region. This can be seen from the plateau that is reached for the Si_2O^+ and $^{30}Si^+$ intensities. The buried steel oxide-APS interface is reached at a sputter dose of 2.17 x 10^{16} ions/cm^2. Based on crater depth measurements by AFM it was determined that the APS coating is approximately 930 nm thick. A detailed description of the procedure for thickness measurements with AFM can be found in supplementary information. In Figure 3, Fe_2O^+ is plotted as a characteristic fragment for the steel oxide surface layer, while Fe_2^+ mainly represents the bulk steel substrate. Remarkable observation is that some nitrogen containing fragments, such as $C_3H_6N^+$ and NH_4^+, show an increase in intensity towards the interface, while other fragments as NH_3^+ do not.
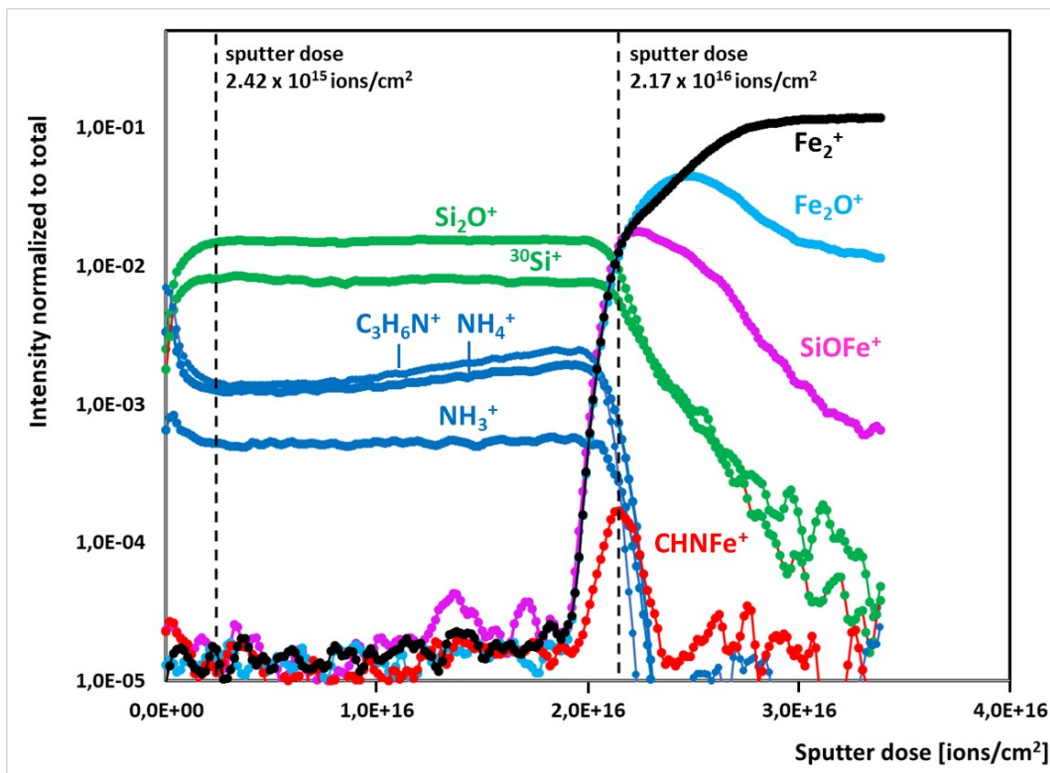

Figure 3: ToF-SIMS depth profile obtained on a spin-coated APS coating on steel.

Figure 3 shows only a small number of fragments (9) that are plotted against sputter dose. A non-negative matrix factorization (NMF) analysis was performed on the depth profile dataset in order to generate components or 'fingerprints' representative for the different chemistries along the depth profile. PCA was performed prior to NMF as an exploratory tool to determine the number of components that should be generated. Details on the PCA analysis can be found in the supplementary information. By PCA it was found that 4 unique chemistries or components could be distinguished in the depth profile (Figure S2); bulk APS coating, surface APS coating, steel oxide - APS interface and steel substrate. Consequently, NMF was performed on the ToF-SIMS depth profile with the constraint that 4 components should be generated. Figure 4 shows the loadings or fingerprint spectra of the 4 NMF components. NMF scores of each component are plotted against sputter dose in Figure 5. Component C1 represents the bulk APS coating accessed by sputtering. Most intense fragments originate from silanol groups and the Si-O-Si network. Component C2 is also representative for the APS coating, but shows increased scores at the outer surface and at the buried interface. Most intense fragments in C2 are nitrogen containing fragments as NH_4^+, CH_4N^+, $C_3H_6N^+$ and $SiC_3H_6N^+$. This suggests that there may be an increased concentration of amine groups at the buried interface and at the outer surface. Component C3 represents the buried interface and contains fragments as $CNFe^+$ and $CHNFe^+$, which suggest amine-steel interactions, but also $SiOFe^+$, SiO_2HFe^+ and $SiO_4HFe_2^+$, which suggests interactions between silanol groups and steel. Finally, component C4 represents the steel substrate as well as the steel oxide surface layer and contains fragments as $^{54}Fe^+$ and Fe_2O^+.
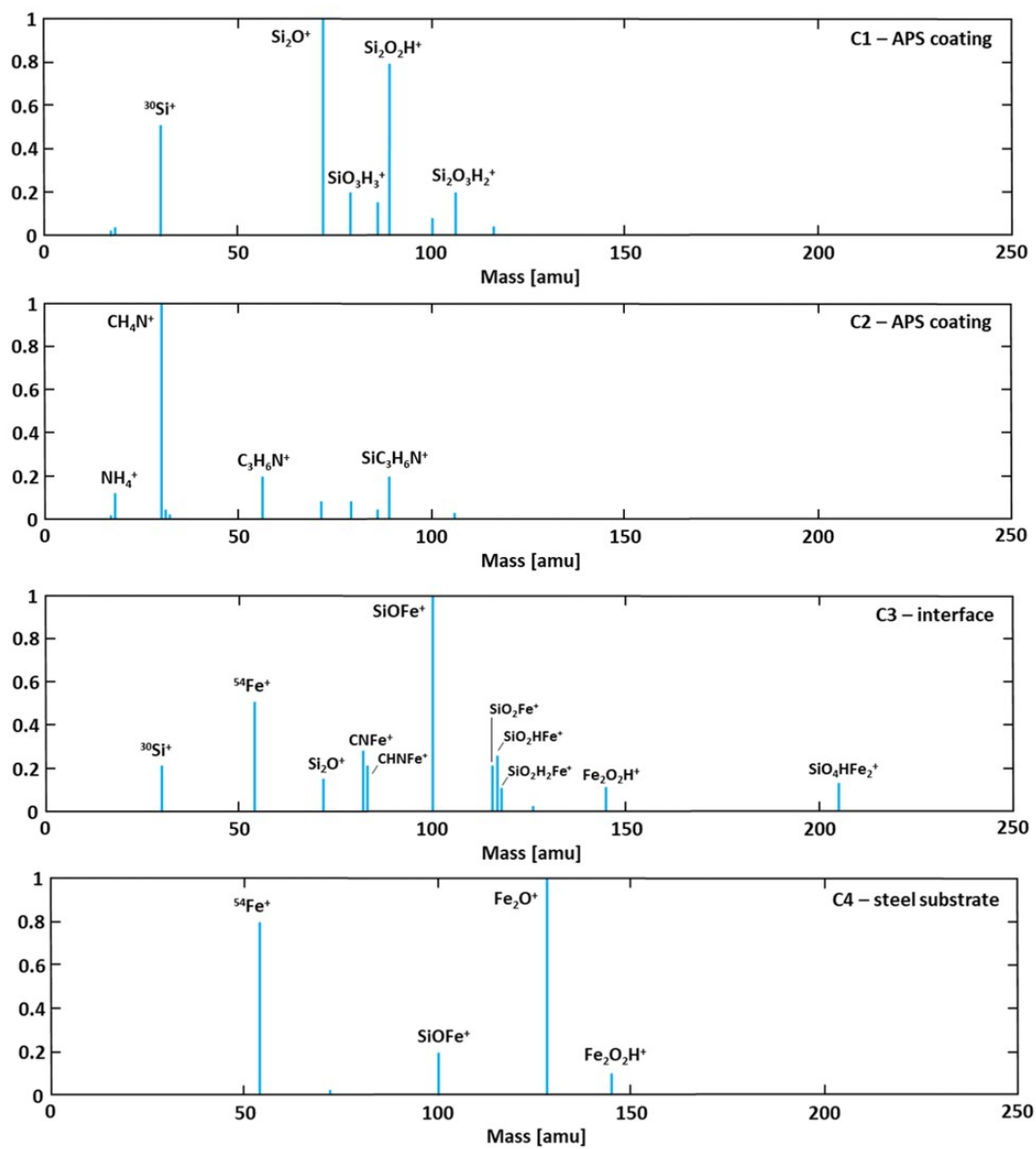
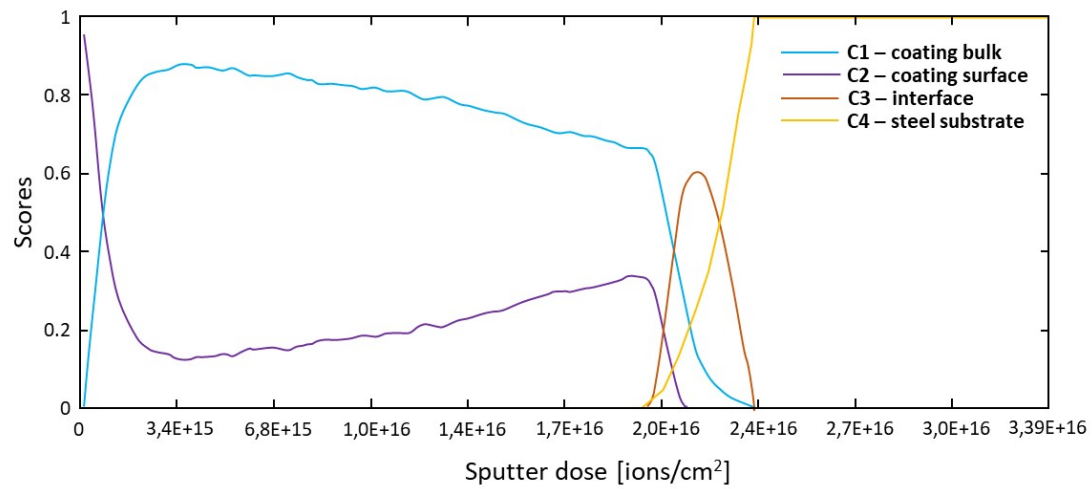Figure 4: NMF fingerprint spectra for components C1-4.

Figure 5: NMF scores for each component plotted against sputter dose. Scores are normalized to the total sum.

3.3   Silanol-steel interactions

Silanol groups interact with steel surface hydroxyl groups initially through hydrogen bonds (Figure 6a). Upon drying or by applying additional heat to the sample, condensation reactions gradually convert hydrogen bonds into stronger covalent Si-O-Fe interactions (Figure 6b). In earlier work it was shown that ToF-SIMS can be applied to characterize both hydrogen bond interactions and covalent bond interactions at the APS-steel interface.[8] This study was performed on steel coated with a thin ($<$ 5 nm) film of APS, where the interface was directly accessible for a ToF-SIMS analysis. Such analysis will be further referred to as a direct interface analysis. Through pre-treatment of steel substrates with NaOD instead of the standard NaOH pre-treatment, steel surface deuteroxide groups are formed instead of surface hydroxyl groups (Figure 6c). Steel surface deuteroxide groups interact with APS silanol groups in the same manner as surface hydroxyl groups (Figure 6d), but yield interesting isotopic fragments in a ToF-SIMS analysis.
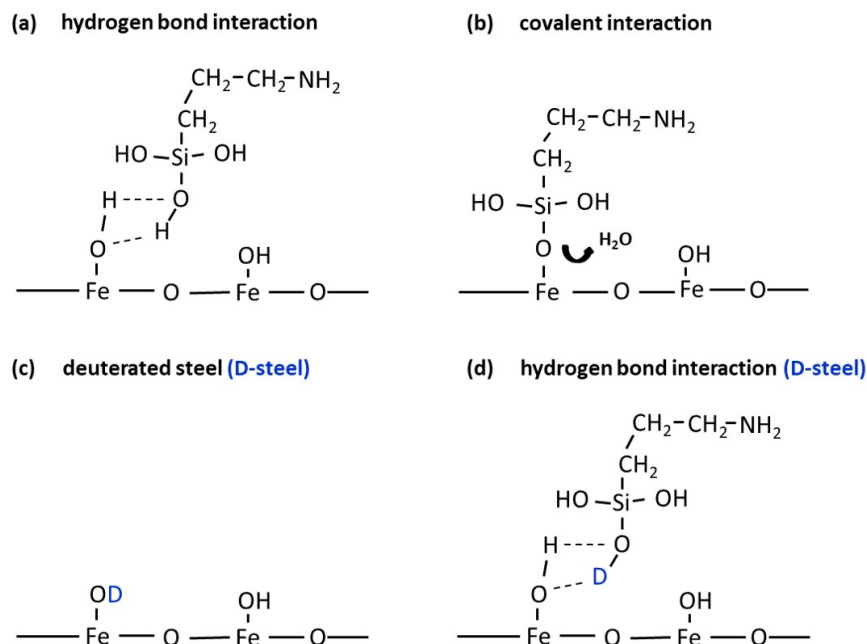

Figure 6: (a) Silanol groups interact with steel surface hydroxyl groups through hydrogen bonding. (b) Covalent Si-O-Fe bonds are formed after a condensation reaction takes place. (c) Deuterated steel surface (D-steel). (d) Hydrogen bond interaction on D-steel.

Deuterated mass fragments that provide unambiguous evidence for hydrogen bond interactions at the steel oxide - APS interface can be extracted from a direct interface analysis by ToF-SIMS. Table 3 summarizes all fragments that were found to be characteristic for hydrogen bond interactions in a direct interface analysis.

Table 3: Ion fragments characteristic for hydrogen bond interactions between silanol groups and steel surface hydroxyl groups, obtained from a direct interface analysis.

Fragment	Mass [ppm]	Deviation [ppm]
$SiOD^+$	45.9849	22.0
$SiO_3H_3^+$	78.9867	26.9
$SiO_3H_2D^+$	79.9908	7.7
$SiO_3H_3Fe^+$	134.9203	5.8
$SiO_3H_2DFe^+$	135.9267	2.5

In Figure 7, the direct interface analysis of the APS-steel interface is compared to a buried interface analysis, in which Ar cluster ions were applied to access the APS-steel interface buried under a thick APS coating. Black spectra were obtained at the direct interface, red spectra were obtained at the buried interface. Figures 7a-b show $SiO_3H_3^+$ and $FeSiO_3H_3^+$, two characteristic fragments for hydrogen bond interactions in the direct interface analysis (Table 3). In the buried interface analysis, $FeSiO_3H_3^+$ is no longer found (Figure 7b). On top of that, none of the deuterated fragments reported in Table 3 were found. The only fragment reported in Table 3 that was found at the buried interface is $SiO_3H_3^+$, but its presence may not originate from hydrogen bond interactions in this case. In the depth profile NMF analysis, $SiO_3H_3^+$ was assigned to the bulk APS coating component C1 (Figure 4). $SiO_3H_3^+$ is a fragment that is characteristic for the bulk APS coating as well as for interfacial hydrogen bond interactions. The $SiO_3H_3^+$ intensity observed in the buried interface analysis is solely attributed to the bulk APS coating. In summary, characteristic mass fragments for hydrogen bond interactions are no longer observed at the buried interface. One must consider that sputter induced damage may be the reason that these fragments are no longer observed, rather than the absence of interfacial hydrogen bond interactions at the buried steel oxide - APS interface.

Figures 7c-d-e-f focus on a number of interfacial fragments that are found at the buried steel oxide-APS interface. $SiOFe^+$, a well-known fragment at the nominal mass 100 u, is measured in a relatively high intensity (Figure 7c). This observation is in line with what has been described in literature. In several studies, $SiOM^+$ fragments (M represents Al, Fe or Zn) have been interpreted as direct evidence for covalent Si-O-M bond formation at the metal oxide-silane interface, both for direct access interfaces[5,40,41] as for buried interfaces.[6,7,42] However, the interpretation that $SiOM^+$ fragments can be considered as proof for covalent bonding has been under discussion.[43] In our analysis, it is remarkable in the NMF analysis (Figure 4) that $SiOFe^+$ is a highly characteristic fragment for the substrate component, as well as for the interface component. Furthermore, when the $SiOFe^+$ intensity is plotted in a depth profile and compared to the $^{54}Fe^+$ intensity (Figure 8a), both profiles show a large resemblance. It seems that the intensity of $SiOFe^+$ is strongly influenced by the concentration of its constituent elements. This suggests that $SiOFe^+$ is formed in the ToF-SIMS experiment due to the impact caused by sputtering. The contribution from interfacial interactions to the $SiOFe^+$ intensity is likely overwhelmed by the contribution from sputter induced damage. Therefore, one should not solely rely on $SiOFe^+$ for a characterization of the buried interface. Larger fragments such as SiO_2Fe^+, SiO_2HFe^+ and $SiO_4HFe_2^+$ are found in both spectra as well (Figures 7d-e-f). All fragments are plotted in a depth profile in Figure 8b, where it becomes clear that these fragments show a much sharper interface as compared to $SiOFe^+$. Especially SiO_2HFe^+ and $SiO_4HFe_2^+$ seem to be highly characteristic for the APS-steel interface and are least influenced by sputter induced damage. At this point, it is possible to state that silanol-steel interactions take place at the buried interface, but unfortunately SiO_2HFe^+ and $SiO_4HFe_2^+$ do not provide enough molecular information to determine whether covalent interactions or hydrogen bond interactions are taking place.
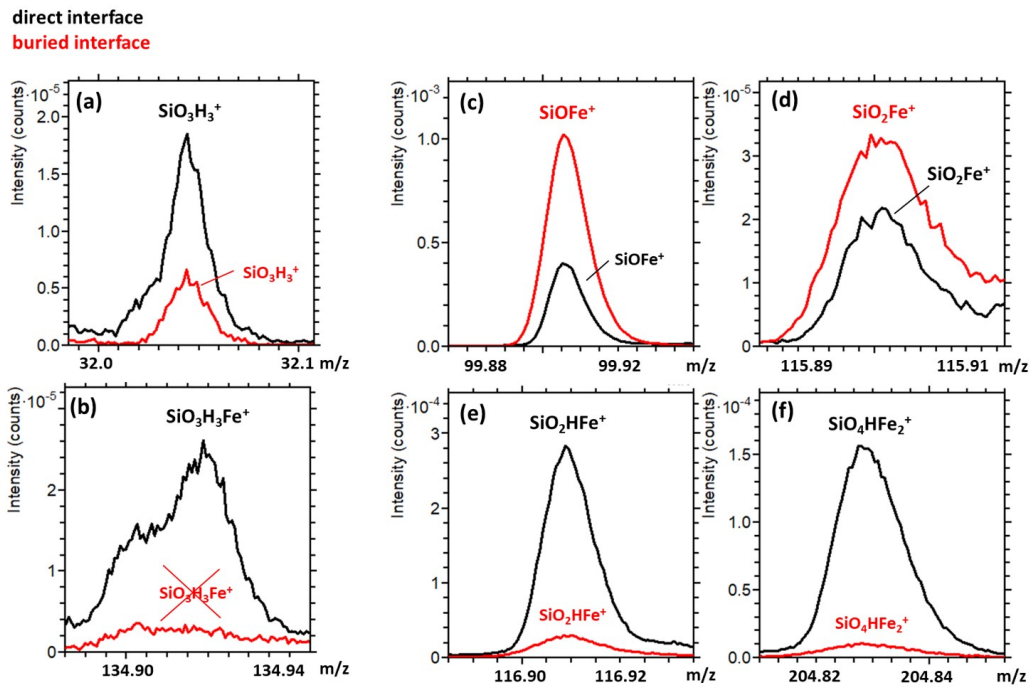
Figure 7: Overlay of ToF-SIMS spectra obtained at the APS-steel interface. The black spectrum was obtained directly on steel coated with a thin film of APS. No sputtering was required to reach the interface. The red spectrum is obtained at the buried APS-steel interface, accessed after sputtering. (a) $SiO_3H_3^+$, (b) $FeSiO_3H_3^+$, (c) $SiOFe^+$, (d) SiO_2Fe^+ and (e) SiO_2HFe^+ and (f) $SiO_4HFe_2^+$.
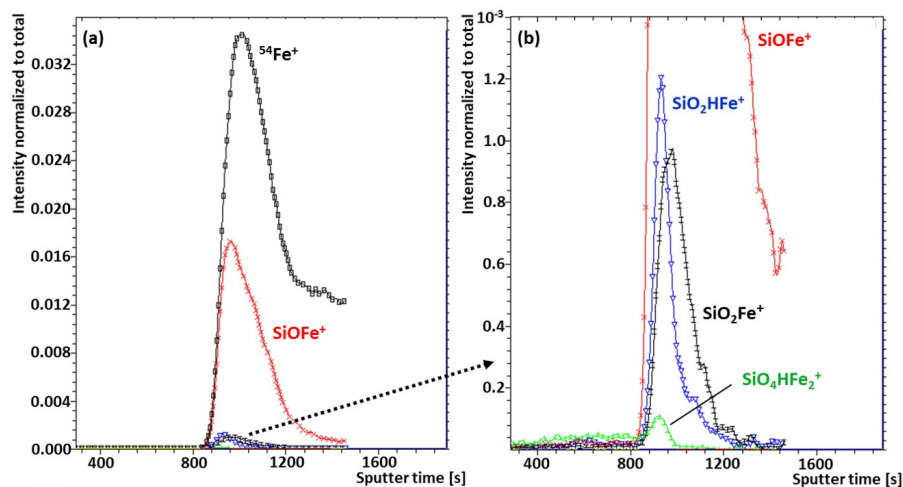

Figure 8: (a) ToF-SIMS depth profile obtained on APS coated steel. The APS-steel interface was reached after approximately 900 s of sputtering . Overlay of $SiOFe^+$ (red) and $^{54}Fe^+$ (black) intensities. (b) Same depth profile as in (a) with a lower intensity scale to pronounce overlay of $SiOFe^+$ (red), SiO_2Fe^+ (black), SiO_2HFe^+ (blue) and $SiO_4HFe_2^+$ (green) intensities.

20

3.4 Amine-steel interactions

Figure 9 makes a comparison between a direct interface analysis and a buried interface analysis at the APS-steel interface. Figures 9a-b-c show interfacial fragments obtained from a ToF-SIMS analysis of a thin APS film on steel. The interface was directly accessible without the need to sputter with an argon GCIB. Figures 9d-e-f show the corresponding mass regions with an overlay of two spectra: the buried APS-steel interface accessed by sputtering (red) and the bulk APS coating accessed by sputtering (black). $CNFe^+$, $CHNFe^+$ and CH_4NFe^+ are fragments characteristic for an acid-base interaction between the APS amine group and steel, found in the direct interface analysis (Figures 9a-b-c). In the buried interface analysis, $CNFe^+$ and $CHNFe^+$ (Figures 9d-e) are still present, but a peak for CH_4NFe^+ is missing (Figure 9f). Either this fragment is no longer formed due to damage induced by sputtering, or its intensity is so small that it is no longer resolved from the neighboring peak, which is attributed to Si_2NO^+.

In the direct interface analysis it was shown that deuteration of steel surface hydroxyl groups allows to distinguish between the different type of amine-steel interactions. Figure 10a shows a ToF-SIMS spectrum overlay of bulk APS in green and the direct APS-steel interface in blue. The latter spectrum was obtained directly, without the need of sputtering, on D-steel coated with a thin ($< 5nm$) APS film. CH_4DN^+ is a fragment indicative for protonation of the APS amine group by steel surface deuteroxide groups and dominates the APS-steel direct interface spectrum at the nominal mass of 32 u. For bulk APS, CH_6N^+ dominates the spectrum at 32 u, while CH_4DN^+ is logically not present. Figure 10b shows a spectrum overlay of a depth profile of APS coated D-steel in red and APS coated H-steel in black. In both profiles, CH_6N^+ dominates the spectrum. However, given the large volume of bulk coating that has been analyzed with respect to the thin interface, it is normal that CH_6N^+ dominates the spectra. Contributions from the interface are relatively small compared to contributions from the bulk coating. Furthermore, the difference in mass between CH_6N^+ and CH_4DN^+ is very small, which makes it difficult to resolve both peaks. Therefore, two
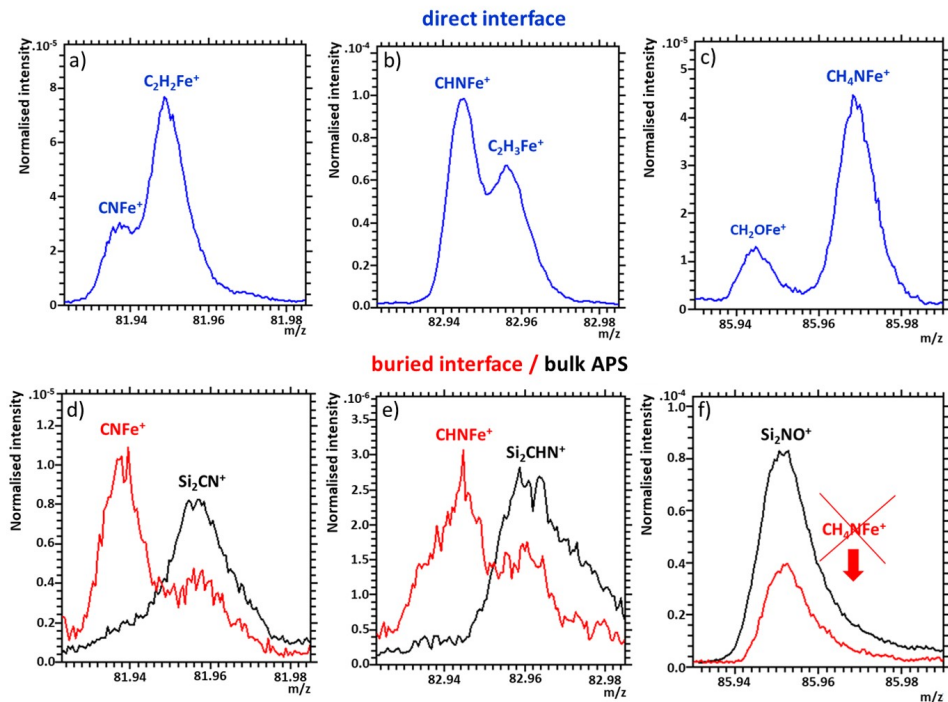
Figure 9: (a-b-c) Interfacial fragments found by a ToF-SIMS analysis of a thin APS film on steel. No sputtering was required, the interface was directly accessible. (d-e-f) Corresponding mass regions showing an overlay of two spectra: the buried APS-steel interface accessed by sputtering (red) and the bulk APS coating accessed by sputtering (black).

mass intervals are selected to be plot in a depth profile. Mass interval I comprises the entire peak area, while mass interval II is limited to the left half of the peak, where CH_4DN^+ could be found. Figures 10c-d show the depth profiles obtained on APS coated D-steel and APS-coated H-steel, respectively. Both profiles were obtained with the same sputter conditions. Since the APS coating was thicker on H-steel, the interface is reached after approximately 450 s of sputtering on H-steel and only 350 s of sputtering on D-steel, as seen by the Fe_2^+ intensity. Mass interval I, comprising the entire CH_6N^+ peak, shows a continuously decreasing intensity in both profiles, although the profile on H-steel decreases more rapidly near the interface. Mass interval II shows an additional contribution at the interface on D-steel, which is absent on H-steel. This contribution on D-steel is attributed to the presence of a CH_4DN^+ at the buried interface. Besides CH_4DN^+, also a peak for NH_3D^+ is found in the depth profile on D-steel. Both peaks are indicating that amine groups at the buried interface are

protonated by steel surface hydroxyl groups. This suggests that amine groups interact with the steel substrate through Brönsted-Lowry acid-base interactions, as illustrated in Figure 11b. $CNFe^+$ and $CHNFe^+$, on the other hand, suggest that Lewis acid-base interactions take place as well (Figure 11a).
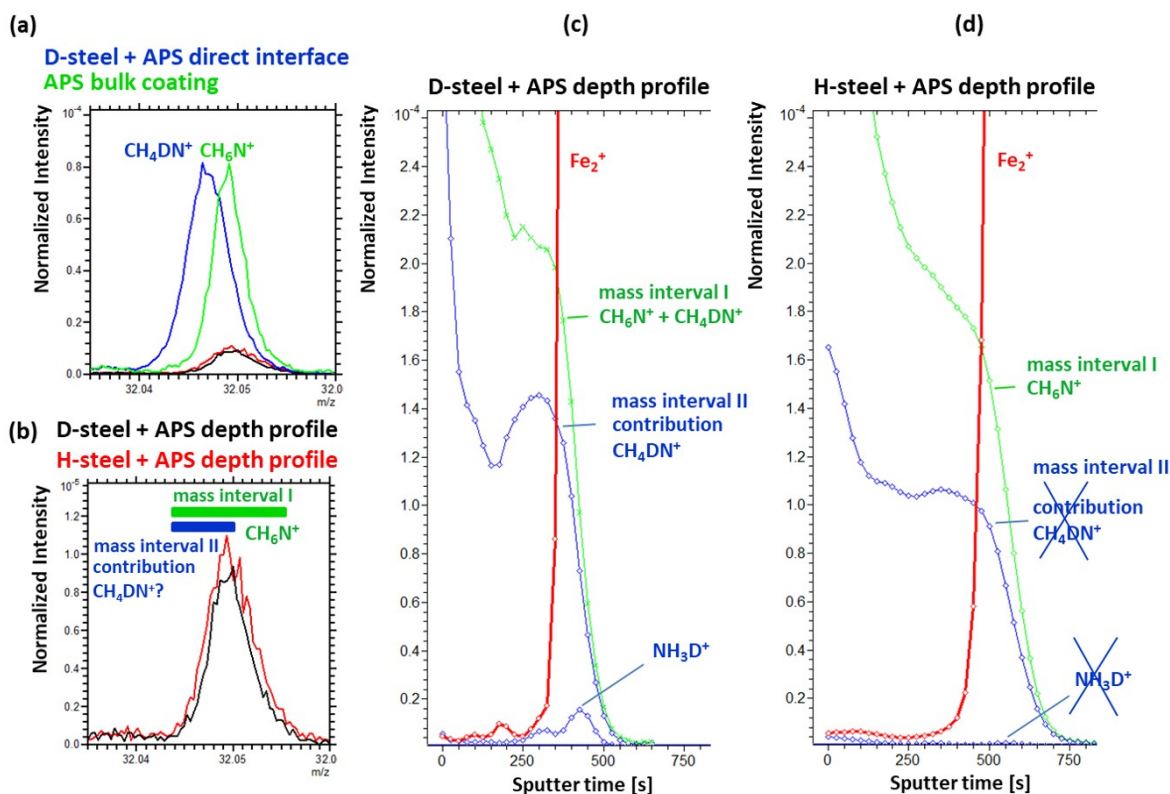

Figure 10: (a) ToF-SIMS overlay showing nominal mass 32 u, where CH_6N^+ and CH_4DN^+ can be interferingly present. The spectrum of a bulk APS coating is shown in green, the steel-APS interface spectrum obtained on APS coated D-steel is shown in blue. Spectra obtained from depth profiles on D-steel coated APS and H-steel coated APS are shown in black and red, respectively. (b) Two mass intervals are defined to be plotted against sputter time in a depth profile, in order to investigate the hidden presence or absence of CH_4DN^+. (c) Depth profile obtained on D-steel coated APS. (d) Depth profile obtained on H-steel coated APS.
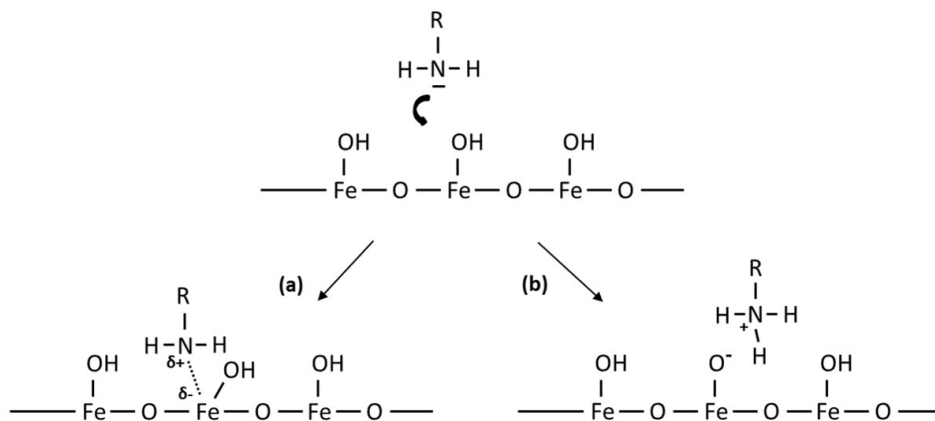
Figure 11: Illustration of the bonding of an amine compound with an iron oxide surface. (a) Lewis acid base interaction (b) Brönsted-Lowry acid-base interaction.

4   Conclusion

An Ar gas cluster ion beam was applied to sputter through APS coatings on steel in order to access the buried steel oxide – silane hybrid interface for a molecular characterization by ToF-SIMS. AFM topography line scans were taken across the sputter crater at different times and under varying sputter conditions, such that the influence of sputtering on sample topography could be evaluated. Optimal sputter conditions were obtained on APS with 10 keV Ar_{1200}^+ settings, corresponding to an E/n of 8.3 eV/atom. Lower E/n values resulted in significant sputter-induced roughness and accumulation of damage during the profile. Mass spectra obtained from the steel oxide – APS interface accessed by Ar cluster sputtering have been compared to spectra obtained from an interface that was directly accessible. This approach demonstrated that there is a significant loss of molecular information due to sputtering. Fragments characteristic for interfacial steel oxide-silanol interactions were extracted at the buried interface, but, unlike fragments obtained in a direct interface analysis, did not provide enough molecular information to determine whether covalent interactions or hydrogen bond interactions take place. This points out the importance of the thin film approach. Despite the loss of molecular interfacial information, mechanistic insights can be still derived in a buried interface analysis. Increased intensities for nitrogen-containing fragments at the

buried steel oxide – APS interface suggest that amine groups tend to orient towards the steel substrate. By deuteration of the steel surface hydroxyl groups it was possible to confirm that this intensity increase originates from a compositional effect, more specifically from Brönsted-Lowry type acid-base interactions between the amine group and steel surface hydroxyl group whereby the amine group becomes protonated.

The present work on model coatings provides an important step towards the analysis of real industrial coating systems, where polymer blends contain multiple polymeric components that can interact with the substrate. Surface and interface segregation effects can play an important role in these systems, as they determine the hybrid interfacial structure. Ultrathin model films cannot represent such phenomena and this explains the necessity to continue the efforts towards analysis of the buried hybrid interface.

Acknowledgement

References

(1) Zaferani, S. H.; Peikari, M.; Zaarei, D.; Danaee, I.; Fakhraei, J. M.; Mohammadi, M. Using silane films to produce an alternative for chromate conversion coatings. *Corrosion* **2013**, *69*, 372–387.

(2) Croll, S.; Vetter, C.; Keil, B. Variability of Pipe Coating Pull-off Adhesion Measurements on Cylindrical Steel Pipelines. *ASCE Pipelines 2012: Innovations in Design, Construction, Operations and Maintenance* **2012**, 231–241.

(3) Ghosh, A. K.; Bertels, E.; Goderis, B.; Smet, M.; Van Hemelrijck, D.; Van Mele, B. Optimisation of wet chemical silane deposition to improve the interfacial strength of stainless steel/epoxy. *Applied Surface Science* **2015**, *324*, 134–142.

(4) Franquet, A.; Biesemans, M.; Terryn, H.; Willem, R.; Vereecken, J. Study of the interaction of hydrolysed silane solutions with pre-treated aluminium substrates. *Surface and Interface Analysis* **2006**, *38*, 172–175.

(5) Gettings, M.; Kinloch, A. J. Surface analysis of polysiloxane/metal oxide interfaces. *Journal of Materials Science* **1977**, *12*, 2511–2518.

(6) Abel, M.; Digby, R. P.; Fletcher, I. W.; Watts, J. F. Evidence of specific interaction between γ-glycidoxypropyltrimethoxysilane and oxidized aluminium using high-mass resolution ToF-SIMS. *Surface and Interface Analysis* **2000**, *29*, 115–125.

(7) Teo, M.; Kim, J.; Wong, P. C.; Wong, K. C.; Mitchell, K. A. R. Investigations of interfaces formed between bis-1, 2- (triethoxysilyl) ethane (BTSE) and aluminum after different Forest Product Laboratory pre-treatment times. *Applied Surface Science* **2004**, *221*, 340–348.

(8) Marcoen, K.; Gauvin, M.; De Strycker, J.; Terryn, H.; Hauffman, T. Molecular Characterization of Multiple Bonding Interactions at the Steel Oxide–Aminopropyl triethoxysilane Interface by ToF-SIMS. *ACS Omega* **2020**, *5*, 692–700.

(9) Abel, M. L.; Rattana, A.; Watts, J. F. Interaction of epoxy analogue molecules with organosilane-treated aluminum: A study by XPS and ToF-SIMS. *Langmuir* **2000**, *16*, 6510–6518.

(10) Van Den Brand, J.; Van Gils, S.; Beentjes, P. C. J.; Terryn, H.; Sivel, V.; De Wit, J. H. W. Improving the Adhesion between Epoxy Coatings and Aluminium Substrates. *Progress in Organic Coatings* **2004**, *51*, 339–350.

(11) Wielant, J.; Hauffman, T.; Blajiev, O.; Hausbrand, R.; Terryn, H. Influence of the iron oxide acid-base properties on the chemisorption of model epoxy compounds studied by XPS. *Journal of Physical Chemistry C* **2007**, *111*, 13177–13184.

(12) Taheri, P.; Hauffman, T.; Mol, J. M. C.; Flores, J. R.; Hannour, F.; de Wit, J. H. W.; Terryn, H. Molecular Interactions of Electroadsorbed Carboxylic Acid and Succinic Anhydride Monomers on Zinc Surfaces. *Journal of Physical Chemistry C* **2011**, *115*, 17054–17067.

(13) Taheri, P.; Wielant, J.; Hauffman, T.; Flores, J. R.; Hannour, F.; De Wit, J. H. W.; Mol, J. M. C.; Terryn, H. A comparison of the Interfacial Bonding Properties of Carboxylic Acid Functional Groups on Zinc and Iron Substrates. *Electrochimica Acta* **2011**, *56*, 1904–1911.

(14) Shimizu, K.; Abel, M. L.; Phanopoulos, C.; Holvoet, S.; Watts, J. F. The characterisation of the interfacial chemistry of adhesion of rigid polyurethane foam to aluminium. *Journal of Materials Science* **2012**, *47*, 902–918.

(15) Tardio, S.; Abel, M. L.; Carr, R. H.; Watts, J. F. The interfacial interaction between isocyanate and stainless steel. *International Journal of Adhesion and Adhesives* **2019**, *88*, 1–10.

(16) Walls, J.; Hall, D.; Sykes, D. Composition-Depth Profiling and Interface Analysis of Surface Coatings using Ball Cratering and the Scanning Auger Microscope. *Surface and Interface Analysis* **1979**, *1*, 204–210.

(17) Watts, J. F. Microbeam analysis applied to adhesion, surfaces and interfaces. *Microchimica Acta* **2009**, *164*, 379–385.

(18) Abel, M. L.; Watts, J. F. Examination of the interface of a model adhesive joint by surface analysis: A study by XPS and ToF-SIMS. *Surface and Interface Analysis* **2009**, *41*, 508–516.

(19) Van Ooij, W.; Kleinhesselink, A. The Application of XPS to the Study of Polymer-Metal Interface Phenomena. *Applications of Surface Science* **1980**, *4*, 324–339.

(20) Shard, A.; Gilmore, I.; Wucher, A. In *ToF-SIMS: Materials Analysis by Mass Spectrometry*, 2nd ed.; Vickerman, J., Briggs, D., Eds.; IM Publications and Surface Spectra Limited, 2013; Chapter 12, pp 311–334.

(21) Mahoney, C. Cluster Secondary Ion Mass Spectrometry of Polymers and Related Materials. *Mass Spectrometry Reviews* **2010**, *29*, 247–293.

(22) Delcorte, A.; Garrison, B. J. keV fullerene interaction with hydrocarbon targets: Projectile penetration, damage creation and removal. *Nuclear Instruments and Methods in Physics Research B* **2007**, *255*, 223–228.

(23) Postawa, Z.; Czerwinski, B.; Szewczyk, M.; Smiley, E. J.; Winograd, N.; Garrison, B. J. Microscopic Insights into the Sputtering of Ag 111 Induced by C_{60}^{+} and Ga Bombardment. *Journal of Physical Chemistry B* **2004**, *108*, 7831–7838.

(24) Yamada, I.; Matsuo, J.; Toyoda, N.; Kirkpatrick, A. Materials processing by gas cluster ion beams. *Materials Science and Engineering R* **2001**, *34*, 231–295.

(25) Rabbani, S.; Barber, A. M.; Fletcher, J. S.; Lockyer, N. P.; Vickerman, J. C. TOF-SIMS with argon gas cluster ion beams: A comparison with C_{60}^{+}. *Analytical Chemistry* **2011**, *83*, 3793–3800.

(26) Wehbe, N.; Tabarrant, T.; Brison, J.; Mouhib, T.; Delcorte, A.; Bertrand, P.; Moellers, R.; Niehuis, E.; Houssiau, L. TOF-SIMS depth profiling of multilayer amino-acid films using large Argon cluster Ar_n^{+}, C_{60}^{+} and Cs^{+} sputtering ions: A comparative study. *Surface and Interface Analysis* **2013**, *45*, 178–180.

(27) Seah, M. P. Universal Equation for Argon Gas Cluster Sputtering Yields. *Journal of Physical Chemistry C* **2013**, *117*, 12622–12632.

(28) Cumpson, P. J.; Portoles, J. F.; Barlow, A. J.; Sano, N.; Birch, M. Depth profiling organic/inorganic interfaces by argon gas cluster ion beams: Sputter yield data for bio-materials, in-vitro diagnostic and implant applications. *Surface and Interface Analysis* **2013**, *45*, 1859–1868.

(29) Noël, C.; Houssiau, L. Hybrid Organic/Inorganic Materials Depth Profiling Using Low Energy Cesium Ions. *Journal of the American Society for Mass Spectrometry* **2016**, *27*, 908–916.

(30) Noël, C.; Busby, Y.; Mine, N.; Houssiau, L. ToF-SIMS Depth Profiling of Organic Delta Layers with Low-Energy Cesium Ions: Depth Resolution Assessment. *Journal of the American Society for Mass Spectrometry* **2019**, *30*, 1537–1544.

(31) Shard, A. G.; Havelund, R.; Seah, M. P.; Spencer, S. J.; Gilmore, I. S.; Winograd, N.; Mao, D.; Miyayama, T.; Niehuis, E.; Rading, D.; Moellers, R. Argon cluster ion beams for organic depth profiling: Results from a VAMAS interlaboratory study. *Analytical Chemistry* **2012**, *84*, 7865–7873.

(32) Tiddia, M.; Mihara, I.; Seah, M. P.; Trindade, G. F.; Kollmer, F.; Roberts, C. J.; Hague, R.; Mula, G.; Gilmore, I. S.; Havelund, R. Chemical Imaging of Buried Interfaces in Organic-Inorganic Devices Using Focused Ion Beam-Time-of-Flight-Secondary-Ion Mass Spectrometry. *ACS Applied Materials & Interfaces* **2019**, *11*, 4500–4506.

(33) Song, J.; Van Ooij, W. J. Bonding and corrosion protection mechanisms of γ-APS and BTSE silane films on aluminum substrates. *Journal of Adhesion Science and Technology* **2003**, *17*, 2191–2221.

(34) Trindade, G. F.; Abel, M. L.; Watts, J. F. simsMVA: A tool for multivariate analysis of ToF-SIMS datasets. *Chemometrics and Intelligent Laboratory Systems* **2018**, *182*, 180–187.

(35) Lee, D. D.; Seung, H. S. Learning the parts of objects by non-negative matrix factorization. *Nature* **1999**, *401*, 788–791.

(36) Berry, M. W.; Browne, M.; Langville, A. N.; Pauca, V. P.; Plemmons, R. J. Algorithms and applications for approximate nonnegative matrix factorization. *Computational Statistics and Data Analysis* **2007**, *52*, 155–173.

(37) Keenan, M. R.; Kotula, P. G. Accounting for Poisson noise in the multivariate analysis of ToF-SIMS spectrum images. *Surface and Interface Analysis* **2004**, *36*, 203–212.

(38) Trindade, G. F.; Abel, M. L.; Watts, J. F. Non-negative matrix factorisation of large mass spectrometry datasets. *Chemometrics and Intelligent Laboratory Systems* **2017**, *163*, 76–85.

(39) Niehuis, E.; Möllers, R.; Rading, D.; Cramer, H. G.; Kersting, R. Analysis of organic multilayers and 3D structures using Ar cluster ions. *Surface and Interface Analysis* **2013**, *45*, 158–162.

(40) Bexell, U.; Olsson, M. Characterization of a non-organofunctional silane film deposited on Al, Zn and Al-43.4Zn-1.6Si alloy-coated steel. *Surface and Interface Analysis* **2001**, *31*, 223–231.

(41) Fang, J.; Flinn, B. J.; Leung, Y. L.; Wong, P. C.; Mitchell, K. A.; Foster, T. A characterization of the γ-glycidoxypropyltrimethoxysilane and aluminium interface by SIMS and XPS. *Journal of Materials Science Letters* **1997**, *16*, 1675–1676.

(42) Batan, A.; Mine, N.; Douhard, B.; Brusciotti, F.; De Graeve, I.; Vereecken, J.; Wenkin, M.; Piens, M.; Terryn, H.; Pireaux, J. J.; Reniers, F. Evidence of covalent bond formation at the silane-metal interface during plasma polymerization of bis-1,2-(triethoxysilyl)ethane (BTSE) on aluminium. *Chemical Physics Letters* **2010**, *493*, 107–112.

(43) Gandhi, J. S.; Singh, S.; Ooij, W. J. V.; Puomi, P. Evidence for formation of metallo-siloxane bonds by comparison of dip- coated and electrodeposited silane films. *Journal of Adhesion Science and Technology* **2006**, *20*, 1741–1768.

Graphical TOC Entry